Temperature Dependence of the Anisotropic Magnetoresistance of the Metallic Antiferromagnet Fe_2As

Junyi Wu,[1,2] Manohar H. Karigerasi,[2,3] Daniel P. Shoemaker,[2,3] Virginia O. Lorenz,[1,2] and David G. Cahill[1,2,3,*]

[1] *Department of Physics, University of Illinois at Urbana-Champaign, 1110 West Green Street, Urbana, Illinois 61801, USA*

[2] *Materials Research Laboratory, University of Illinois at Urbana-Champaign, Urbana, Illinois 61801, USA*

[3] *Department of Materials Science and Engineering, University of Illinois at Urbana-Champaign, Urbana, Illinois 61801, USA*

(Received 18 November 2020; revised 4 March 2021; accepted 16 April 2021; published 18 May 2021)

Electrical readout of metallic antiferromagnet (AFM) memories is typically realized by measuring the anisotropic magnetoresistance (AMR), but the mechanisms for enhanced AMR are not yet established. We study AMR of single crystals of AFM Fe_2As from $T = 5$ K to above the Néel temperature, $T_N \approx 353$ K. With an applied magnetic field B rotating in the (001) plane, we observe a peak-to-peak AMR change of 1.3% for $B > 1$ T at $T = 5$ K, one order of magnitude larger than reported in CuMnAs, a widely studied candidate for AFM spintronics. The AMR varies strongly with temperature, decreasing by a factor of approximately 10 at $T \approx 200$ K. Our results suggest that large AMR in easy-plane AFMs may require Néel temperatures that greatly exceed room temperature.

DOI: 10.1103/PhysRevApplied.15.054038

I. INTRODUCTION

Antiferromagnetic materials have great potential in next-generation spintronic devices. Their attractive properties include the absence of stray fields, insensitivity to external fields, and terahertz-frequency spin dynamics [1–3]. A key challenge of antiferromagnetic spintronics is finding an efficient method for determining the magnetic order parameter, i.e., the orientation of the Néel vector. One method to determine the orientation of the Néel vector is by measuring the anisotropic magnetoresistance (AMR). AMR has been used in the past for readout in ferromagnetic memory [4], and widely used in magnetic field sensors [5]. AMR is an even function of magnetization and is therefore also present in antiferromagnets [6].

In this work, we use the term AMR to refer to the effect of the orientation of the Néel vector on the electrical resistance of an antiferromagnet (AFM). Therefore, the dominant mechanism of AMR in a metallic AFM is distinct from ordinary magnetoresistance (OMR), i.e., the effect of the orientation of the magnetic field on the resistance of a metal. In OMR, an external field perpendicular to the current leads to a longer current path and larger resistivity. The magnitude of OMR in typical metals scales as $(\mu B)^2$, where μ is the electrical mobility [7]. Since the mobility of our Fe_2As is small, of the order of 3 $cm^2\ V^{-1}\ s^{-1}$ at low temperatures [8], conventional OMR should be negligible in our samples.

A large, approximately 4%, AMR in Cr was observed 50 years ago by comparing the resistivity parallel and perpendicular to the Néel vector of a single domain sample created by cooling through the Néel temperature in a strong magnetic field [9]. (The domain wall magnetoresistance of Cr has also been quantified [10].) The emergence of AFMs as potential memory elements has motivated a large number of experimental and theoretical studies of AMR in metallic and semiconducting AFMs in recent years [6,11,12]. The AMR of Sr_2IrO_4 is 10% [11,12].

Fe_2As is a metallic conductor and therefore comparisons to other metallic AFMs are most relevant. The systems that have received the most attention are FeRh, Mn_2Au, and CuMnAs. FeRh with a small excess of Rh is predicted to have an AMR of 1.5% [13]. FeRh is among the few materials that have a transition between ferromagnetic and antiferromagnetic order as a function of temperature. This behavior enables the control of the Néel vector orientation by cooling through the transition temperature in an easily accessible magnetic field of 1 T [13]. The measured value of the AMR is of the order of 0.3% at $T = 200$ K and 1% at 80 K. In the thin-film samples of FeRh studied by Marti *et al.* [13], the orientation of the Néel vector in the AFM phase is preserved even when exposed to strong magnetic fields of 9 T. The resistance is not independent of the orientation of the 9 T magnetic field rotating in the

*d-cahill@illinois.edu

plane of the sample, but the changes in resistance are much smaller, of the order of 0.1% at $T = 200$ K, than the AMR that derives from the orientation of the Néel vector relative to the current direction [13].

The AFM domain texture and AMR of Mn_2Au has been studied extensively. Mn_2Au was predicted from first principles to have a high Néel temperature with easy-plane magnetocrystalline anisotropy [14,15]. This magnetic behavior was later confirmed by neutron diffraction [16]. In 2018, Bodnar *et al.* [17] calculated the AMR of Mn_2Au for both the hard ⟨100⟩ and easy ⟨110⟩ directions as a function of disorder and found AMR as large as 6% for compositions with excess Au in the hard direction. In 2020, Bodnar *et al.* [18] reported a thorough study of magnetoresistance of Mn_2Au in pulsed magnetic fields of strength up to 60 T. The authors concluded that a field of 30 T is needed to form a single antiferromagnetic domain and that the AMR in the easy direction is approximately 0.15%. As was the case for FeRh thin films [13], it has not yet been possible to observe AMR in Mn_2Au produced by the rotation of the Néel vector in response to a rotating magnetic field. Polycrystalline samples of Mn_2Au created from bulk ingots, however, do not show hysteresis in the magnetic susceptibility [16]; the reversibility of the magnetic susceptibility implies that Mn_2Au prepared from the melt may have domain structures that are easier to manipulate than the domain structures in thin-film materials created by sputter deposition.

The chemical and magnetic structure of Fe_2As is closely related to the structure of CuMnAs. Wang *et al.* [19] reported AMR with twofold symmetry reaching 0.5% at $T = 2$ K in 50 nm thick tetragonal antiferromagnetic CuMnAs epitaxial layers. The AMR decreases to 0.3% at room temperature. The CuMnAs film was grown on a GaP(001) substrate with the hard magnetic axis normal to the surface. Volný *et al.* [20] studied bulk CuMnAs in the tetragonal phase, reporting a 0.12% magnitude twofold AMR signal with an applied field of $B = 6$ T that decreases slightly with temperature between 5 and 400 K.

Fe_2As is a tetragonal collinear AFM with globally centrosymmetric but locally noncentrosymmetric magnetic structure [21]. A metallic AFM with these symmetry elements, such as CuMnAs [22–24] and Mn_2Au [17], have been shown to have potential to be switched electrically. Moreover, Fe_2As, CuMnAs, and M_2Au are "easy-plane" AFMs: the spin magnetic moments lie in the (001) plane with two degenerate orientations. Yang *et al.* [25] recently measured the in-plane fourfold magnetocrystalline anisotropy of a millimeter-size bulk crystal of Fe_2As by torque magnetometry and found an extremely small easy-plane anisotropy of 150 J/m^3 at $T = 4$ K. A relatively small applied field of $B \approx 2$ T was found to be sufficient to form a single domain at room temperature.

In this work, we characterize the magnitude of the AMR response in metallic millimeter-sized single crystals of Fe_2As as a function of temperature and applied magnetic field. The use of single-crystal samples minimizes extrinsic effects created by inhomogeneous strain and high densities of extended defects that are common in thin-film materials. In the low-temperature limit, $T \approx 5$ K, the AMR response reaches 1.3%. The AMR response decreases to 0.04% at room temperature and falls to near zero at the Néel temperature (approximately 353 K). The temperature dependence of the AMR response differs qualitatively from that of the electrical resistivity or the square of the sublattice magnetization, indicating that other quantities play a role in determining the temperature dependence of AMR in Fe_2As.

We contrast our findings for Fe_2As with what has been observed in epitaxial layers of CuMnAs [19]. In both Fe_2As and CuMnAs, a field strength of $B < 1$ T is sufficient to saturate the AMR signal. However, Fe_2As displays an AMR signal at low temperatures, $T < 50$ K, that is an order of magnitude larger than CuMnAs. The strong temperature dependence of the AMR signal we observe in Fe_2As is not observed in CuMnAs [19] or typical ferromagnetic alloys [26].

II. EXPERIMENT

Fe_2As single crystals are synthesized by mixing Fe and As powders and vacuum sealing the starting materials in a fused quartz tube. The quartz tube is heated at 1 °C/min to 600 °C and held for 6 h in a furnace. The temperature is then ramped to 975 °C at 1 °C/min and held for 1 h before cooling to 900 °C at 1 °C/min. Finally, the quartz tube is kept at 900 °C for 1 h and allowed to cool to room temperature in the furnace at 10 °C/min or, for selected samples, at 1 °C/min. We obtained large silver-hued crystals of Fe_2As. From previous studies described in Ref. [21], Fe_2As samples are known to be slightly off-stoichiometric, with Fe deficiency of 0.05 to 0.08 out of 2, evaluated using Rutherford backscattering spectrometry and Rietveld refinements to x-ray and neutron diffraction data. The defects that create the off-stoichiometry are not yet known but antisite defects (As on Fe sites) are likely candidates. The defects that are responsible for the off-stoichiometry are also the likely cause of the large residual electrical resistivities of our samples.

We use a wire saw to cut Fe_2As crystals into approximately 200-μm-thick plates with surfaces parallel to the (001) planes of the crystal. Fe_2As slices are polished down to 80 μm thickness with diamond lapping films from 9, 3, 1 μm down to 0.1 μm. X-ray diffraction pole figures are performed after polishing. The miscut of the samples away from the (001) orientation of the crystal is less than 10°.

To prepare a substrate for the measurements of AMR, we deposit four 200 × 200 μm^2 200-nm-thick Au contact pads on a 1.5 × 2 cm^2 fused quartz plate. The Fe_2As slices are attached to this substrate with epoxy. We wire bond the

Fe_2As along the [100] orientation at four points, approximately 200 μm apart, to the contact pads. The wire bonds use 25 μm diameter, approximately 2 mm long 1% Al:Si wire. The misalignment of the current direction relative to the crystallographic axis is less than 12°. The Fe_2As sample and substrate are mounted to a sample holder puck with silver paint. We then wire bond the sample from the contact pads to electrodes of the sample holder puck. The resistance of the individual wire bonds is about 1 Ω. The resistance of the sample is measured by a four-point method.

Temperature and magnetic-field-dependent AMR measurements are performed in a Quantum Design physical property measurement system (PPMS). We use the horizontal sample rotator of the PPMS to control the angle between the crystal and the applied magnetic field. During the measurement, the sample is rotated in the applied field in the (001) easy plane. Probing currents of 3 mA are applied along the [100] direction, corresponding to a current density of 2×10^3 A cm^{-2}. Typical switching current densities for similar materials, e.g., CuMnAs and Mn_2Au, are at least 5000 times higher [27]. We record the longitudinal resistance change along the [100] crystal direction, $\Delta R = R - \overline{R}$, where $\overline{R}$ is the average resistance over the full sweep of the orientation of the applied magnetic field in the (001) plane.

We prepared five samples from four growth runs: 1, 2a, 2b, 3, and 4, in which 2a and 2b are from the same growth run. We cooled sample 4 to room temperature at a lower rate of 1 °C/min. We measured the room-temperature electrical resistivity of all samples using a four-point probe with probe spacing 200 μm. The uncertainty in the four-point probe measurement is 15%. The geometry factor A/L of the wire-bonded sample used in the PPMS measurements is found by comparing the room-temperature resistance R measured in the PPMS system to the room-temperature resistivity ρ measured by the four-point probe, $A/L = \rho/R$. The PPMS measurements of resistance are converted to resistivity using $\rho(T) = R(T)(A/L)$.

III. RESULTS AND DISCUSSION

The Fe_2As single crystals have resistivities of the order of 100 $\mu\Omega$ cm; see Fig. 1. Our results are similar to previously reported measurements of Fe_2As polycrystals [28, 29]. The samples studied by Takeshita *et al.* [29], however, show a larger relative change between high temperatures and low temperature, i.e., larger residual resistance ratio, than our samples or the samples studied by Zocco *et al.* [28]. At $T < 10$ K, the resistivity is constant. The resistivity increases with temperature for $T > 30$ K, presumably due to an increasing rate of electron-phonon scattering, and approaches a plateau near room temperature.

The residual resistivity of sample 1 is a factor of approximately 2 larger than the residual resistivity of the other samples. We are unsure of the origin of this difference and tentatively assign the higher residual resistivity of sample 1 to a higher density of antisite defects, associated with deviations from stoichiometry. Sample 4 has about a 25% smaller residual resistivity than samples 2a, 2b, and 3. We attribute this difference to the factor of 10 slower cooling rate for this sample.

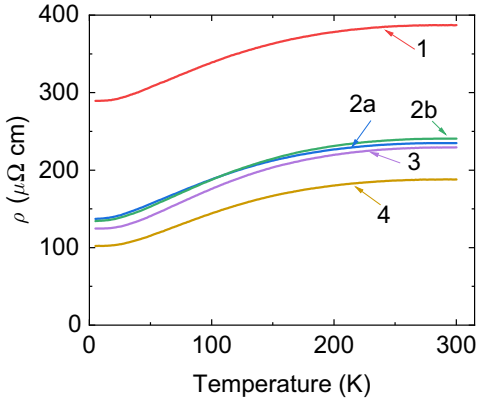

FIG. 1. Temperature dependence of the electrical resistivity of Fe_2As along the ⟨100⟩ orientation for five different samples, labeled as 1, 2a, 2b, 3, and 4.

We characterize the AMR of our samples by the change in the longitudinal resistivity normalized by the average resistivity $\Delta\rho/\overline{\rho}$; see Fig. 2. The change in resistivity is positive when the field is perpendicular to the current direction. With increasing field strength, the AMR increases and saturates at applied fields above 1 T. At high fields, the Néel vector is perpendicular to the applied field; therefore, the resistivity is at a maximum when the current direction is in the same direction as the Néel vector. The change in resistance is well described by a $\Delta\rho \propto \cos(2\theta)$ dependence, where θ is the angle between the magnetic field and the current direction.

During an angular sweep of the applied magnetic field, we do not observe significant hysteresis of the AMR response. This is in contrast to the hysteresis in the domain structures of a 10 nm CuMnAs film at 200 K [19], where hysteresis of the order of 20% was observed. The lack of hysteresis in our measurements suggests that our single-crystal Fe_2As samples have fewer or weaker domain pinning sites. On the timescale of our AMR measurements, an equilibrium domain structure is established by the magnetic field that drives the domains toward a single orientation and random strains in the crystal that drive the domains toward a disordered structure [30]. (We discuss the reversibility of the AFM domain structure in more detail below.)

For a typical tetragonal crystal, the angular dependence of AMR can be described by a phenomenological model [31]. The resistivity of the sample depends on the relative

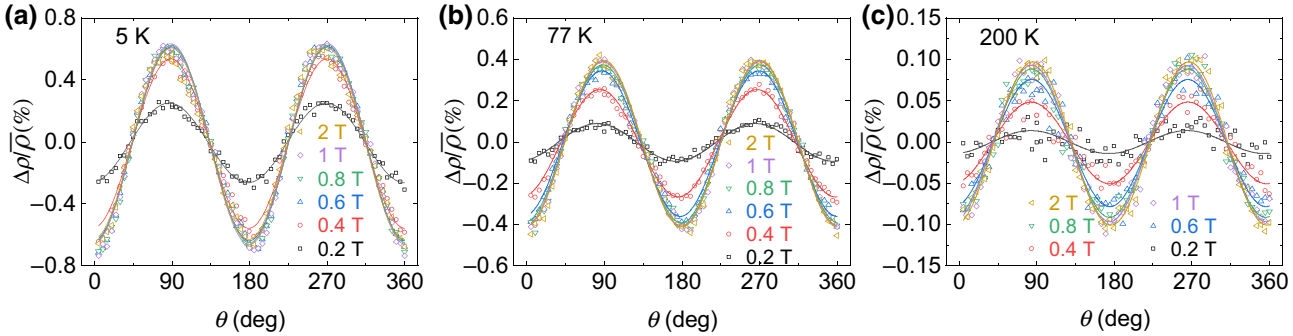

FIG. 2. Change in the longitudinal resistivity $\Delta\rho/\overline{\rho}$ of Fe_2As as a function of the strength and orientation of the applied magnetic field for sample 2a; θ is the angle between the applied field and the current direction. The magnetic field is rotating in the (001) plane of the crystal. The electrical current is in the [100] direction. The three panels summarize data for three sample temperatures: (a) $T = 4$ K, (b) $T = 77$ K, and (c) $T = 200$ K. Open symbols are measured data labeled by the strength of the magnetic field; solid lines are fits to the data of the functional form $\Delta\rho/\overline{\rho} \propto \cos 2\theta$.

orientation of the Néel vector, the magnetic field direction, the current direction, and the crystal axes. Because of the symmetry of the crystal, there are twofold and fourfold contributions to the AMR. We fix the current direction along the [100] direction of the crystal by the placement of the wire-bonded contacts. In the high-field limit where the orientation of the Néel vector is approximately perpendicular to the magnetic field, the change of resistivity is

$$\frac{\Delta\rho}{\rho} = (C_I + C_u)\cos(2\phi) + C_c\cos(4\phi). \qquad (1)$$

The angle ϕ describes the relative orientation of the Néel vector and the direction of the electrical current; C_I is the noncrystalline contribution. The crystalline contributions, C_u and C_c, correspond to the twofold and fourfold symmetries in the (001) plane.

We analyze the AMR data by fitting the oscillations of $\Delta\rho/\rho$ as a function of ϕ to twofold and fourfold contributions with the amplitude and phase of the twofold and fourfold terms as free parameters. The fit of this model to the data is shown as solid lines in Fig. 2. At all temperatures, the amplitude of the twofold contributions is an order of magnitude larger than the fourfold contribution. The fourfold signal has a small shift in phase relative to the twofold signal; see Table S2 within the Supplemental Material [32].

We do not yet understand the origin of the small phase shift between the twofold and fourfold contributions to the AMR signal. There are two potential misalignment angles in our experiment: misalignment between the current direction and the angular position of the sample rotator; and misalignment between the current direction and the [100] direction of the crystal. We tentatively assign the phase shift to a systematic error in the direction of the current, i.e., the placement of the wire-bonded contacts, relative to the [100] direction of the crystal.

The peak-to-peak amplitude of the twofold contribution to the AMR signal $\Delta\rho/\overline{\rho}$ is plotted as a function of the applied field in Fig. 3. The AMR signal approaches a constant value at applied fields larger than a saturation field B_s

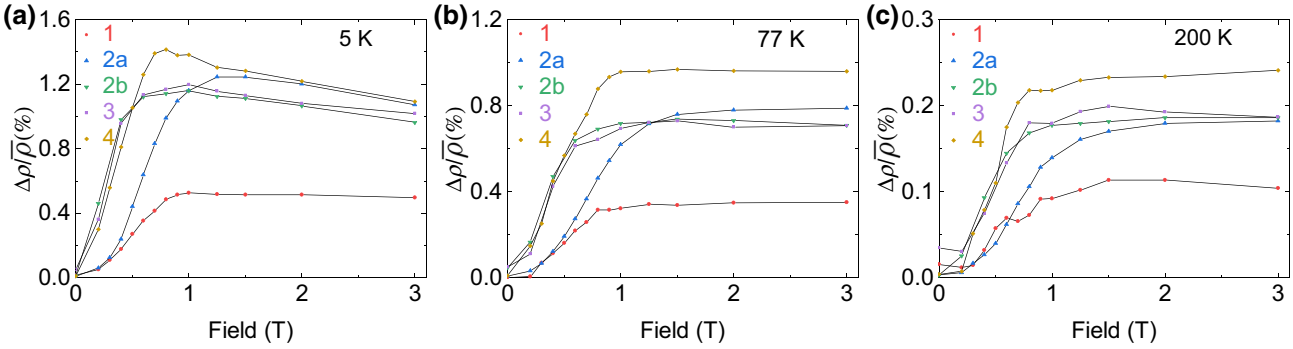

FIG. 3. Magnetic field dependence of the anisotropic magnetoresistance of Fe_2As at (a) 5 K, (b) 77 K, and (c) 200 K for the five samples. The y axis is the peak-to-peak amplitude of the relative change in resistivity for the magnetic field parallel and perpendicular to the current direction.

that is of the order of 1 T. We attribute sample-to-sample variations in B_s to differences in defect microstructures and stoichiometries between the five samples.

Our previous torque magnetometry measurements of Fe_2As [25] reveal an abrupt change in the sign of the torque for applied fields $B > 1$ T rotating in the (010) plane, i.e., rotating between the easy plane and the hard axis. This abrupt change in torque implies that an applied field of $B > 1$ T orients the Néel vector perpendicular to the applied field. As the applied field moves towards and is aligned to the c axis, the populations of the two domains become equal again.

Based on our previous work [25] and the lack of hysteresis in our AMR measurements, we thus conclude that the domain structure of our Fe_2As crystals is reversible. The reversibility of AFM domains has been observed in other AFM materials and the attempt to explain these observations has a long history [33]. Gomonay and coworkers [34,35] proposed a theoretical description based on the intrinsic mismatch of magnetoelastic effects at the bulk and surface of the crystal. We speculate, however, in agreement with Corliss *et al.* [30], that the reversibility of the domain structure in our samples is caused by a combination of relatively weak in-plane magnetocrystalline anisotropy [25] and the magnetoelastic coupling between the orientation of the Néel vector and random strains that are produced by small variations in composition, the concentrations of point defects, or the presence of dislocations.

The observation of a saturation field of $B_s \sim 1$ T in the AMR data (Fig. 3) is consistent with this interpretation of the torque data [25]. In a zero field, we expect that the Néel vector of different magnetic domains does not have a preferred direction and therefore the effect of the Néel vector orientation on the resistivity averages to zero. As the field strength increases, the sublattice magnetization aligns perpendicular to the applied field to minimize the total energy. When the field strength exceeds a saturation field $B_s \sim 1$ T, the Néel vector is approximately perpendicular to the applied field.

In addition to the AMR response that is due to the effect of B on the orientation of the Néel vector, we observe a significant isotropic increase of approximately 1.5% in the electrical resistivity at fields up to $B = 9$ T; see Fig. S1 within the Supplemental Material [36]. We do not emphasize the high-field behavior here and can only speculate that this large isotropic MR effect is due to the influence of strong magnetic fields on defect states [37].

Figure 4 shows the temperature dependence of the twofold contribution to AMR at a field of $B = 3$ T, approximately a factor of 2 larger than the typical saturation field. The overall temperature dependence of the AMR signal is similar for all five samples. The AMR ratio decreases with increasing temperature until it vanishes near the Néel temperature, as expected for an AMR signal associated with magnetic order. In the low-temperature limit, at $T = 5$ K,

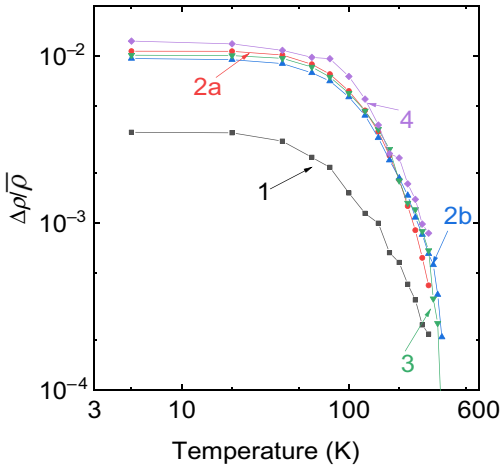

FIG. 4. The AMR signal at $B = 3$ T as a function of temperature for the five samples. The y axis is the peak-to-peak amplitude of the relative change in resistivity as a function of the magnetic field direction.

the peak-to-peak amplitude of the AMR signal reaches 1.3%. Thus, Fe_2As displays AMR signals that are an order of magnitude larger than bulk [20] CuMnAs (0.12%) and epitaxial layers [19] of CuMnAs (0.15%).

The AMR signal decreases rapidly with increasing temperature at $T > 100$ K. Previous neutron scattering data of Fe_2As show that the sublattice magnetization decreases by only 15% between 50 and 200 K [38]. Hence, the strong temperature dependence of the AMR signal cannot be interpreted as due to the sublattice magnetization alone.

Compared with AMR observed in ferromagnets and ferromagnetic alloys, AMR of Fe_2As has a much stronger temperature dependence [39]. Typically, for metal alloys, the dominant scattering mechanism changes from electron-defect scattering to electron-phonon scattering with increasing temperature and the AMR at low temperatures is larger than the AMR at high temperatures [26].

The strong temperature dependence of AMR in Fe_2As is apparently unique among previously studied easy-plane metallic AFMs. (Strong temperature-dependent AMR however is observed in semiconductor Sr_2IrO_4, where large spin-orbit interactions enable band structure changes at low temperature [40].) AMR data for bulk samples of tetragonal metallic AFM CuMnAs do not show a significant temperature dependence between 5 and 400 K [20]. AMR data for relatively thick epitaxial layers of CuMnAs show only a modest decrease of less than a factor of 2 between 2 K and room temperature [19].

IV. CONCLUSION

Through measurement of anisotropic magnetoresistance, we find that external fields less than 1 T are sufficient to reversibly change the orientation of the Néel vector

within the easy plane of the tetragonal metallic antiferromagnet Fe_2As. In the low-temperature limit, the change in resistivity produced by the rotation of the Néel vector is greater than 1%. The AMR signal is, however, strongly temperature dependent and decreases abruptly with increasing temperature at $T > 100$ K. This strong temperature dependence has not been observed in AMR of ferromagnets or the metallic antiferromagnet CuMnAs [19,20] and suggests that the exceptionally large AMR response in Fe_2As at low temperatures has a different physical origin. Since the AMR signal falls rapidly at temperatures above 1/3 of the Néel temperature, our data for Fe_2As suggest that large AMR in easy-plane AFMs for operation at room temperature may require Néel temperatures that exceed 900 K.

ACKNOWLEDGMENTS

This research is supported by the NSF through the University of Illinois at Urbana-Champaign Materials Research Science and Engineering Center DMR-1720633. This work was carried out in part in the Materials Research Laboratory Central Research Facilities, University of Illinois.

[1] V. M. Gomonay and E. V. Loktev, Spintronics of antiferromagnetic systems, Low Temp. Phys. **40**, 17 (2014).
[2] T. Jungwirth, X. Marti, P. Wadley, and J. Wunderlich, Antiferromagnetic spintronics, Nat. Nanotechnol. **11**, 231 (2016).
[3] V. Baltz, A. Manchon, M. Tsoi, T. Moriyama, T. Ono, and Y. Tserkovnyak, Antiferromagnetic spintronics, Rev. Mod. Phys. **90**, 015005 (2018).
[4] T. McGuire and R. Potter, Anisotropic magnetoresistance in ferromagnetic 3d alloys, IEEE Trans. Magn. **11**, 1018 (1975).
[5] J. Heremans, Solid state magnetic field sensors and applications, J. Phys. D: Appl. Phys. **26**, 1149 (1993).
[6] D. Kriegner, K. Vỳbornỳ, K. Olejník, H. Reichlová, V. Novák, X. Marti, J. Gazquez, V. Saidl, P. Němec, V. V. Volobuev, G. Springholz, V. Holý, and T. Jungwirth, Multiple-stable anisotropic magnetoresistance memory in antiferromagnetic MnTe, Nat. Commun. **7**, 1 (2016).
[7] A. B. Pippard, *Magnetoresistance in Metals* (Cambridge University Press, New York, 1989), Vol. 2.
[8] Kisung Kang and André Schleife, Private communications.
[9] W. Muir and J. Ström-Olsen, Electrical resistance of single-crystal single-domain chromium from 77 to 325 K, Phys. Rev. B **4**, 988 (1971).
[10] R. Jaramillo, T. F. Rosenbaum, E. D. Isaacs, O. G. Shpyrko, P. G. Evans, G. Aeppli, and Z. Cai, Microscopic and Macroscopic Signatures of Antiferromagnetic Domain Walls, Phys. Rev. Lett. **98**, 117206 (2007).
[11] C. Wang, H. Seinige, G. Cao, J.-S. Zhou, J. B. Goodenough, and M. Tsoi, Anisotropic Magnetoresistance in Antiferromagnetic Sr_2IrO_4, Phys. Rev. X **4**, 041034 (2014).
[12] H. Wang, C. Lu, J. Chen, Y. Liu, S. Yuan, S.-W. Cheong, S. Dong, and J.-M. Liu, Giant anisotropic magnetoresistance and nonvolatile memory in canted antiferromagnet Sr_2IrO_4, Nat. Commun. **10**, 1 (2019).
[13] X. Marti, *et al.*, Room-temperature antiferromagnetic memory resistor, Nat. Mater. **13**, 367 (2014).
[14] S. Khmelevskyi and P. Mohn, Layered antiferromagnetism with high néel temperature in the intermetallic compound Mn_2Au, Appl. Phys. Lett. **93**, 162503 (2008).
[15] A. B. Shick, S. Khmelevskyi, O. N. Mryasov, J. Wunderlich, and T. Jungwirth, Spin-orbit coupling induced anisotropy effects in bimetallic antiferromagnets: A route towards antiferromagnetic spintronics, Phys. Rev. B **81**, 212409 (2010).
[16] V. Barthem, C. Colin, H. Mayaffre, M.-H. Julien, and D. Givord, Revealing the properties of Mn_2Au for antiferromagnetic spintronics, Nat. Commun. **4**, 1 (2013).
[17] S. Y. Bodnar, L. Šmejkal, I. Turek, T. Jungwirth, O. Gomonay, J. Sinova, A. Sapozhnik, H.-J. Elmers, M. Kläui, and M. Jourdan, Writing and reading antiferromagnetic Mn_2Au by néel spin-orbit torques and large anisotropic magnetoresistance, Nat. Commun. **9**, 348 (2018).
[18] S. Y. Bodnar, Y. Skourski, O. Gomonay, J. Sinova, M. Kläui, and M. Jourdan, Magnetoresistance Effects in the Metallic Antiferromagnet Mn_2Au, Phys. Rev. Appl. **14**, 014004 (2020).
[19] M. Wang, *et al.*, Spin flop and crystalline anisotropic magnetoresistance in CuMnAs, Phys. Rev. B **101**, 094429 (2020).
[20] J. Volný, D. Wagenknecht, J. Železný, P. Harcuba, E. Duverger-Nedellec, R. H. Colman, J. Kudrnovský, I. Turek, K. Uhlířová, and K. Výborný, Electrical transport properties of bulk tetragonal CuMnAs, Phys. Rev. Mater. **4**, 064403 (2020).
[21] K. Yang, K. Kang, Z. Diao, A. Ramanathan, M. H. Karigerasi, D. P. Shoemaker, A. Schleife, and D. G. Cahill, Magneto-optic response of the metallic antiferromagnet Fe_2As to ultrafast temperature excursions, Phys. Rev. Mater. **3**, 124408 (2019).
[22] P. Wadley, B. Howells, J. Zelezny, C. Andrews, V. Hills, R. Campion, V. Novak, F. Freimuth, Y. Mokrousov, A. Rushforth, K. W. Edmonds, B. L. Gallagher, and T. Jungwirth, Electrical switching of an antiferromagnet, Science **351**, 587 (2016).
[23] J. Godinho, H. Reichlová, D. Kriegner, V. Novák, K. Olejník, Z. Kašpar, Z. Šobáň, P. Wadley, R. P. Campion, R. Otxoa, and P. E. Roy, Electrically induced and detected néel vector reversal in a collinear antiferromagnet, Nat. Commun. **9**, 1 (2018).
[24] T. Matalla-Wagner, M.-F. Rath, D. Graulich, J.-M. Schmalhorst, G. Reiss, and M. Meinert, Electrical Néel-Order Switching in Magnetron-Sputtered CuMnAs Thin Films, Phys. Rev. Appl. **12**, 064003 (2019).
[25] K. Yang, K. Kang, Z. Diao, M. H. Karigerasi, D. P. Shoemaker, A. Schleife, and D. G. Cahill, Magnetocrystalline anisotropy of the easy-plane metallic antiferromagnet Fe_2As, Phys. Rev. B **102**, 064415 (2020).
[26] L. Berger, P. P. Freitas, J. D. Warner, and J. E. Schmidt, On the temperature dependence of the magnetoresistance of ferromagnetic alloys, J. Appl. Phys. **64**, 5459 (1988).

[27] O. J. Amin, K. W. Edmonds, and P. Wadley, Electrical control of antiferromagnets for the next generation of computing technology, Appl. Phys. Lett. **117**, 010501 (2020).

[28] D. A. Zocco, D. Y. Tütün, J. J. Hamlin, J. R. Jeffries, S. T. Weir, Y. K. Vohra, and M. B. Maple, High pressure transport studies of the LiFeAs analogs $CuFeTe_2$ and Fe_2As, Supercond. Sci. Technol. **25**, 084018 (2012).

[29] N. Takeshita, A. Iyo, S. Ishida, H. Eisaki, and Y. Yoshida, Electrical resistivity of FeAs, $FeAs_2$ and Fe_2As at homogeneous high pressures, J. Phys.: Conf. Ser. **950**, 042024 (2017).

[30] L. M. Corliss, J. M. Hastings, W. Kunnmann, R. J. Begum, M. F. Collins, E. Gurewitz, and D. Mukamel, Magnetic phase diagram and critical behavior of Fe_2As, Phys. Rev. B **25**, 245 (1982).

[31] A. W. Rushforth, K. Výborný, C. S. King, K. W. Edmonds, R. P. Campion, C. T. Foxon, J. Wunderlich, A. C. Irvine, P. Vašek, V. Novák, K. Olejník, J. Sinova, T. Jungwirth, and B. L. Gallagher, Anisotropic Magnetoresistance Components in (Ga, Mn)As, Phys. Rev. Lett. **99**, 147207 (2007).

[32] See Supplemental Material at http://link.aps.org/supplemental/10.1103/PhysRevApplied.15.054038 for a discussion of the fitted AMR coefficient.

[33] B. Tanner, Antiferromagnetic domains, Contemp. Phys. **20**, 187 (1979).

[34] H. Gomonay and V. M. Loktev, Magnetostriction and magnetoelastic domains in antiferromagnets, J. Phys.: Condens. Matter **14**, 3959 (2002).

[35] E. Gomonay and V. Loktev, On the theory of the formation of equilibrium domain structure in antiferromagnets, Low Temp. Phys. **30**, 804 (2004).

[36] See Supplemental Material at http://link.aps.org/supplemental/10.1103/PhysRevApplied.15.054038 for a discussion of the behavior of the magnetoresistance for fixed magnetic field directions at high fields.

[37] S. Tsunashima, G. Bayreuther, and H. Hoffmann, Anisotropic magnetoresistance of amorphous Fe–Zr alloy films, Jpn. J. Appl. Phys. **29**, 529 (1990).

[38] H. Katsuraki and N. Achiwa, The magnetic structure of Fe_2As, J. Phys. Soc. Jpn. **21**, 2238 (1966).

[39] R. P. van Gorkom, J. Caro, T. M. Klapwijk, and S. Radelaar, Temperature and angular dependence of the anisotropic magnetoresistance in epitaxial Fe films, Phys. Rev. B **63**, 134432 (2001).

[40] I. Fina, X. Marti, D. Yi, J. Liu, J. Chu, C. Rayan-Serrao, S. Suresha, A. Shick, J. Železnỳ, T. Jungwirth, F. Fontcuberta, and R. Ramesh, Anisotropic magnetoresistance in an antiferromagnetic semiconductor, Nat. Commun. **5**, 1 (2014).